Power exhaust scenarios for EU-DEMO

PAPER • OPEN ACCESS

Power exhaust scenarios for EU-DEMO

To cite this article: F. Subba *et al* 2025 *Nucl. Fusion* **65** 086024

OPEN ACCESS
IOP Publishing | International Atomic Energy Agency
Nuclear Fusion
Nucl. Fusion **65** (2025) 086024 (14pp)
https://doi.org/10.1088/1741-4326/adeac2

Power exhaust scenarios for EU-DEMO

F. Subba[1,*], **W. Van Uyten**[2] **and S. Wiesen**[3]

[1] NEMO Group, Politecnico di Torino, Torino, Italy
[2] KU Leuven, Department of Mechanical Engineering, Leuven, Belgium
[3] DIFFER, Eindhoven, Netherlands

E-mail: fabio.subba@polito.it

Received 19 March 2025, revised 23 June 2025
Accepted for publication 2 July 2025
Published 18 July 2025

Abstract

We present an analysis of possible power exhaust scenarios for EU-DEMO. We employ the SOLPS-ITER code with the newly developed advanced fluid neutral model to scan a relatively wide range of neutral pressure divertor and impurity concentration in the core to test the existence of a suitable finite-extension operational space. Ideally, such a region should provide low target power fluxes, negligible erosion, high He divertor compression, and low impurity core concentration. Within the approximations of our model, we identified a non empty region where this long set of constraints can be satisfied. Here we use the constraints $q_{\max} \leqslant 10\,\mathrm{MWm}^{-2}$, $Z_{\mathrm{eff}} \leqslant 1.2$ and $T_{\mathrm{e}} \leqslant 5\,\mathrm{eV}$, the latter being a proxy for detachment. This region corresponds to an upstream density within the range $n_{\mathrm{e,up}} = 0.5 - 0.7\,n_{\mathrm{e,GW}}$ (large but not necessarily prohibitive), Ar separatrix concentration $\leqslant 10^{-3}$ and divertor neutral pressure ranging from 40 to 50 Pa. This is encouraging, in view of a more detailed analysis to be performed on the best-performance area.

Keywords: EU-DEMO, power exhaust, SOLPS-ITER, operational space

(Some figures may appear in color only in the online journal)

1. Introduction

EU-DEMO is the proposed demonstrative fusion reactor prototype on which Europe is focusing its efforts as the next major step following ITER. It has the main goal of demonstrating the possibility of supplying electrical power to the grid while producing *in-situ* a sufficient amount of tritium to sustain continuous operations.

To achieve a proper machine lifetime, it is of paramount importance to guarantee that all components directly exposed to the harsh plasma environment are subject to tolerable energy and particle fluxes. Currently accepted heat flux limits are about $1\,\mathrm{MWm}^{-2}$ [1] onto the main wall chamber and $10\,\mathrm{MWm}^{-2}$ onto the divertor region [2]. At the same time, an electron temperature $T_{\mathrm{e}} \leqslant 5\,\mathrm{eV}$ is desirable to prevent sputtering from eroding too much wall material, which could (i) lead to dangerous core impurity accumulation and (ii) limit the divertor lifetime itself. Injecting a sufficient amount of extrinsic medium-Z impurities (e.g. Ar) could allow, in principle, radiating $\geqslant 90\%$ of the plasma heating power. This could trigger divertor detachment and meet the above requirements [3]. However, poor divertor screening could lead to excessive core impurity penetration, degrading the reactor performance. This adds further constraints to an already multi-dimensional problem.

Designing a machine capable of meeting these requirements is a complex task, which cannot rely on available experimental data only. Present or near-term machines can reproduce some of the EU-DEMO expected parameters, but not all of them [4]. This is why theoretical predictions are expected to give a significant contribution, complementing the available databases and extrapolating them to reactor-relevant regimes. Several modeling efforts are ongoing to fill this gap. They span not only the standard SN divertor configuration, but cover

* Author to whom any correspondence should be addressed.

also alternative solutions [5, 6]. Previous work focused on standard SN has suggested the possibility of obtaining acceptable divertor conditions with a standard single null configuration, relying on Ar impurity injection [7]. However, that work examined only a single operational point; more extensive studies are required to robustly identify a possible area for reactor operations.

Here, we present a more extended systematic study of the EU-DEMO divertor and upper Scrape-off Layer plasma, performed with the SOLPS-ITER code [8]. As explained later, the current work is based on a more recent magnetic equilibrium than [7]. This might still change in the future, to further optimize the machine performances. Then, we believe the work performed on previous and current releases will provide a valuable basis to speed-up updated analysis, which moreover is not expected to result in dramatic conclusion changes. We focus on high upstream density to favor divertor detachment, aiming at maximizing the neutral pressure while controlling the core impurity penetration. We successfully identify conditions of low target heat fluxes and acceptable Ar core concentration. This is promising in view of more refined studies, which can contribute to finalizing the EU-DEMO design.

The paper is organized as follows. Section 2 recalls the main physical parameters expected for EU-DEMO, with a focus on the implications for our study. Section 3 discusses the setup selected for the subsequent modeling. Then, section 4 describes the parametric study performed, scanning several values of the neutral pressure and Ar core concentration to identify a suitable operational region. Later, section 5 discusses in detail one of the most favorable obtained scenarios, as an example of what the EU-DEMO plasma could look like, and to help pointing out the way towards further developments. Finally, in section 6 we wrap-up our main results and discuss possible future developments.

2. Physical setup

EU-DEMO is, at the current state, a partially work in progress design. Project parameters are not yet fully consolidated. Instead, they are still being revised, to incorporate the latest knowledge aiming at achieving maximum machine performance and reliability. To perform our study, we selected a configuration produced in 2021. It is an evolution of the plasma equilibrium assumed in [7] for which no official publication exists [4]. By post-processing the geometrical and magnetic data we determined the major and minor radii to be $R_0 = 9.46$ m and $a = 2.87$ m, respectively, with plasma current $I_p = 18.2$ MA and Greenwald density $n_{GW} = 7.0 \cdot 10^{19}$ m^{-3}.

The L–H transition threshold can be estimated as $P_{LH} \approx 130$ MW [9]. In our modeling it is convenient to set the input power P_{in} at the computational mesh core boundary, which is located several cm inside the separatrix (Outer Mid Plane location), see figure 1. To be consistent with H-mode operation, we conservatively set $P_{in} = 150$ MW. In EU-DEMO the total heating power is estimated to be $P_{heat} = P_\alpha + P_{aux} \approx 450$ MW [10]. That means that roughly 300 MW should be radiated in the plasma column periphery. It is usually assumed that this should be obtained by injecting in the plasma a suitable amount of an extrinsic species optimized to radiate at edge core temperatures. Considering $T \approx 100$ eV at the separatrix, a medium-Z material, e.g. Xe, is thought to be a promising candidate [11]. However, we do not include it in our model, to not exceed the available computational power. This should still be kept in mind when discussing our results, especially in terms of core impurity contamination.

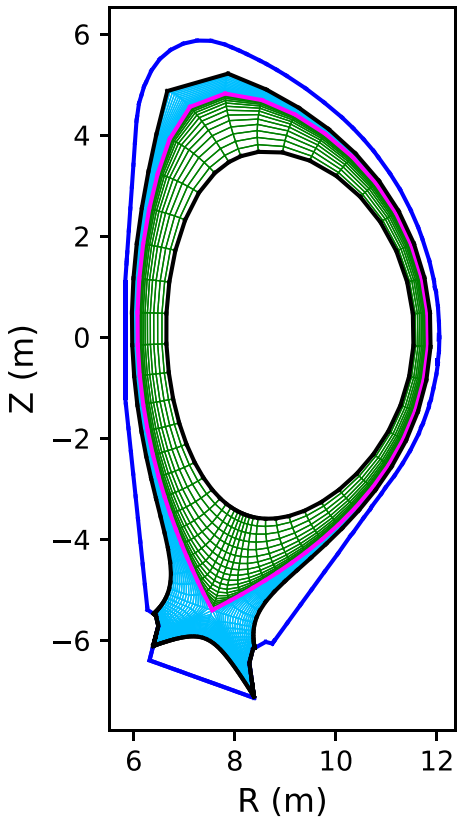

Figure 1. Computational model geometry and mesh. As a guide to the eye, the plot also shows the LCFS (magenta) and the profile of the wall chamber (blue). Different mesh colors distinguish the core (green) from the SOL and divertor regions (light blue).

We consider a plasma composed by D (taken here as proxy for a D–T mixture), He, which is intrinsically present, because it is produced by the fusion reactions themselves, and Ar (selected as SOL radiator). Fuel is fed at the outer wall (for simplicity we assume the influx to be uniformly distributed), and is pumped out from the divertor. The Deuterium particle balance strongly influences the electron density, via quasi-neutrality. In turn, the latter interacts in the SOL with Ar, which dissipate power through radiation and feed-back controls how much energy is left to sustain the recycling regime. This complex interplay ultimately determines the upstream

[4] The reader with access to the EUROFusion Integrated Document Management (IDM) System can find a description of the EU-DEMO design point referred to in this paper at https://idm.euro-fusion.org/?uid = 2NT5PD.

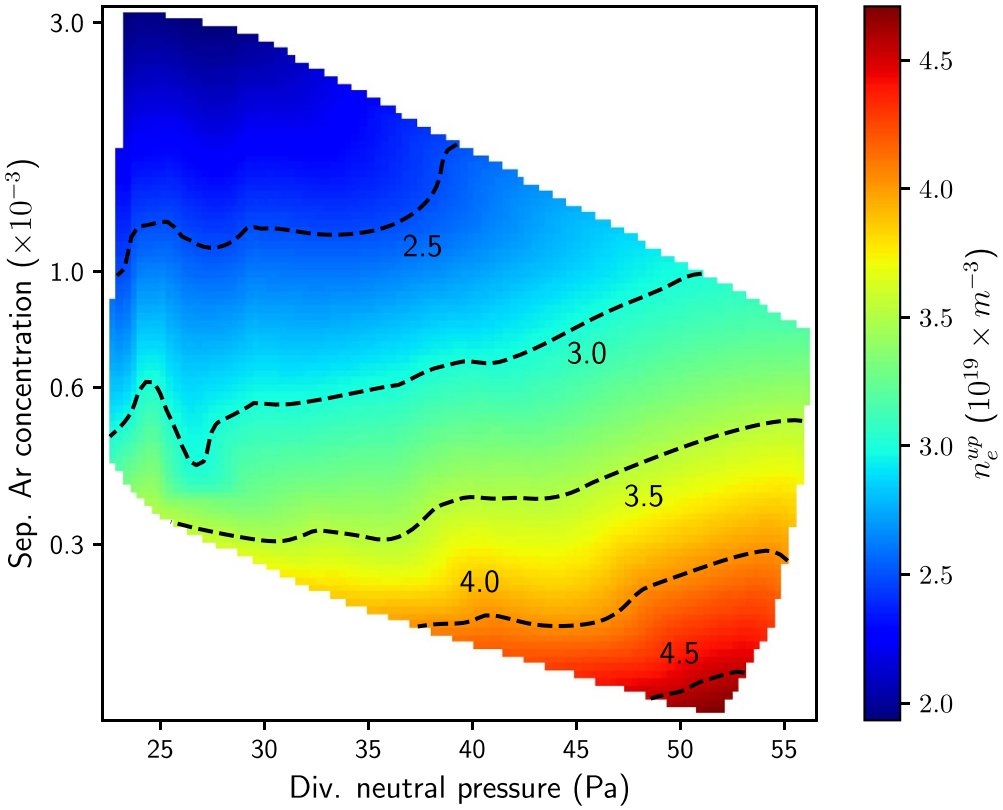

Figure 2. Upstream density ($10^{19} \times \mathrm{m}^{-3}$) obtained for the operational space explored.

density, see later the discussion of figure 2. Ar injection (through the outer wall) is forward-controlled, leading to separatrix concentrations in the range $0.13 \cdot 10^{-3} - 3 \cdot 10^{-3}$. The corresponding upstream density varies from $1.9 \cdot 10^{19}$ to $4.7 \cdot 10^{19}\,\mathrm{m}^{-3}$. He^{2+} is injected at the core boundary at a constant rate of $7.1 \cdot 10^{20}\,\mathrm{s}^{-1}$, consistently with the assumed fusion power $P_{\mathrm{fus}} = 2\,\mathrm{GW}$. While we cannot define a hard limit to its accumulation in the core, it is clear that its presence should be kept the lowest possible for optimum fusion performance. In section 4 we will discuss the overall core impurity presence in more detail. A potentially strong contribution to the reactor energy balance could be triggered by atoms sputtered from the wall, expected to be made of W. On the other hand, previous estimates suggest that the low target temperature required for target protection should also effectively suppress W sputtering [12]. For this reason, we assumed that including W would not displace dramatically the boundary of a reactor-relevant operational region, and decided to drop it from our current calculations.

3. Numerical modeling

The SOLPS-ITER code allows the user to finely tune the desired physical model. Specifically, for this study we selected the newly released so-called *wide-grid* version. We did not yet leverage its main capability to extend dramatically the computational domain in the far SOL because, when the work was started, the grid generation for fully extended cases was not yet mature. However, the new code version also implements additional physics model which can strongly enhance its efficiency, as discussed in [13]. We did rely on such new features, as well as on other critical numerical improvements. For example, it was shown in [13] that the 9-point stencil discretization is absolutely essential to get accurate results with fluid neutrals, and this is now active by default in the wide grid version. Moreover, work on efficient development of good quality extended grids is developing fast [14, 15]; we deemed convenient to start gaining experience in using this new code version.

In principle, SOLPS-ITER allows reproducing in great details the major physical processes taking place in a tokamak edge plasma. However, it is common experience that convergence on large size machines can be difficult and time consuming. Several acceleration techniques are being developed, like e.g. [16]. Here we choose a somewhat aggressive approach, allowing many simplifications to afford exploring a reasonably extended operational space in a limited amount of time. We aim here at identifying a first set of approximate parameters, which should be later the subject of more detailed analysis. It is worth briefly presenting the main assumptions made, to allow the reader an informed evaluation of the later results.

3.1. Neutral transport

It is commonly accepted that SOLPS-ITER produces the most accurate analysis of divertor conditions when the Monte-Carlo (MC) EIRENE module is employed to analyze neutral

transport. However, the MC technique introduces statistical noise and, especially for highly collisional regimes requires long computational times. To mitigate these problems, we activated the advanced fluid neutral (AFN) model for all our cases [14]. The AFN model implements boundary conditions and transport coefficients consistent with the kinetic approach in a neutral gas fluid model, eliminating statistical noise and reducing drastically the required computational time. The fluid approach was shown to be accurate for high-density cases, while being less effective in low-recycling conditions. This is not a major drawback, however. In fact, high-recycling or detached regimes are the ones relevant for EU-DEMO operations. Still, caution should be adopted because the model does not yet include molecular hydrogen. Indeed, deuterium will be puffed in the system, so it will enter the plasma chamber in molecular form; several studies shows that it may play a role in strongly detached divertor plasmas [17, 18]. Moreover, the AFN model is currently only applicable to the main fuel species (D in our case), while impurities are treated with the less accurate default fluid neutral approximation.

3.2. Drifts

This work aims at exploring the EU-DEMO operational domain to point out the presence of acceptable performance regions, with no need to analyze accurately the optimal condition. Though drifts can affect the divertor performance details [2], we do not expect the global picture to be overly sensible to their influence. Consequently, we did not include them in our simulations, obtaining a simpler numerical model. Some recently developed acceleration techniques exist with potential to obtain similar performances even with drifts included [19]. However, these have not yet been fully tested in connection with the AFN model and the related, deeply renewed, internal code structure. From previous experience on ITER studies, we know that including drifts could somehow shrink the admissible divertor operational space [2, 19]. Therefore, we plan to activate them at a later stage, when we will conduct more detailed analyses on a reduced set of plasma conditions.

3.3. Electric currents and potential equation

Drift implementation is tightly related to an accurate description of electric field in the SOL and related currents. Having decided to neglect the former, the latter also becomes less critical. We took advantage of this, and decided to adopt the aggressively simplified approximation $\phi = 3.1\,T_e/q_e$. Our experience shows that this results in a sensible improvement of the code stability. That obviously implies reduced accuracy related, e.g. to the representation of current-driven energy flux or thermo-electrical currents [20, 21].

4. Parametric study results

In this section we analyze a database of 22 SOLPS-ITER runs, aiming at detecting the presence of a possible acceptable operational space, defined in terms of power target deposition, detachment onset and core impurity accumulation. Figure 2 shows the upstream density, as a function of the divertor neutral pressure and separatrix Ar concentration. Lacking the geometrical details of the full chamber representation, and not including molecular deuterium in our simulations, we need to define how to exactly evaluate the neutral pressure. We decided to take the average pressure of D_0 atoms taken along the private flux boundary computational domain. This definition will be consistently adhered to in figures 2–10 below. The expected SOL screening effect at high plasma densities is apparent, with Ar concentration reducing by more than one order of magnitude while the upstream density raises from $\approx 1.9 \cdot 10^{19}$ to $\approx 4.7 \cdot 10^{19}$ (m^{-3}) reaching $\approx 67\%$ of the Greenwald limit. The latter value is larger than the $n_{GW} \leqslant 0.5$ condition sometimes assumed for optimal confinement performance [22]. Here, we speculate that what really matters is the level at the pedestal top, so that our separatrix value can still be marginally acceptable, depending on the exact density profile across the edge.

A key parameter to assess the actual capacity to obtain the desired regime is given by the required pumping speed. We estimated it as

$$S_{pump} \approx \frac{\Gamma_{D,wall}}{n_{D,pfr}} \tag{1}$$

with $\Gamma_{D,wall}$ being the deuterium flux fueled at the wall, and $n_{D,pfr}$ the neutral D density averaged at the private flux boundary. Results are given in figure 3. Values are higher than what is usually suggested by detailed pumping analysis, which usually do not exceed a few tens $m^3\,s^{-1}$ [23, 24]. However, it should be pointed out that we included several simplifications in our modeling, which might directly affect the pumping speed estimate. In particular, (i) our representation of the wall geometry in the divertor region is strongly simplified, (ii) we still assume a fluid model for neutrals, and (iii) we do not include molecules in our study. These pumping speed values should then be considered as indicative, and used to consistently compare cases within the present discussion, but not adopted for a more extensive assessment.

We discuss target conditions by focusing on the electron temperature and power flux deposition at the outer plate. T_e is relevant because it strongly influences possible sputtering, while q_{tar} sets the active cooling system requirements. So, these are quantities with a direct engineering influence. The outer target selection is motivated by the observation that we observed it to be the critical one in our study. Figures 4 and 5 show the peak power flux density on the outer target (including electron and ion heat fluxes, kinetic and recombination energy) and maximum electron temperature. In the latter, an island structure of high peak temperature in the lower-left corner can be identified. There is no obvious physical reason for the development of such feature, which one can also observe in several other pictures; we attribute it to the data interpolation procedure required to produce the operational space plot. When the analysis of an extended region leverages on a relatively sparse data set, the appearance of similar artifacts can be expected.

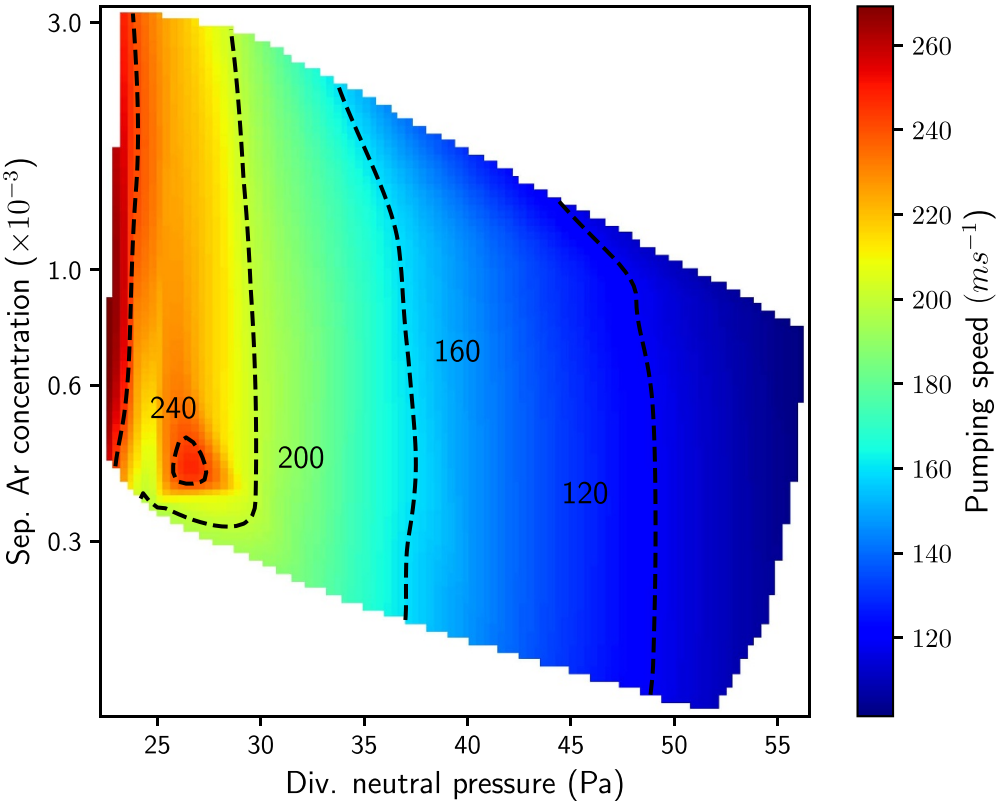

Figure 3. Pumping speed ($m^3\,s^{-1}$) evaluated at the private flux boundary.

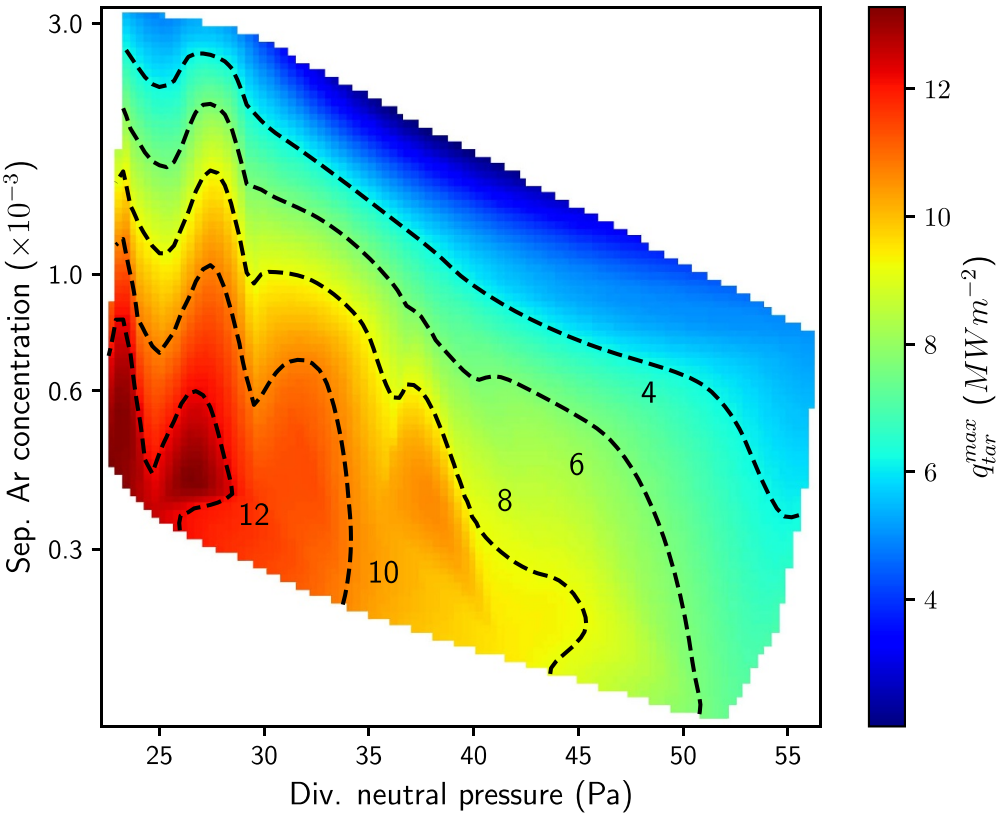

Figure 4. Maximum outer target power flux ($MW\,m^{-2}$).

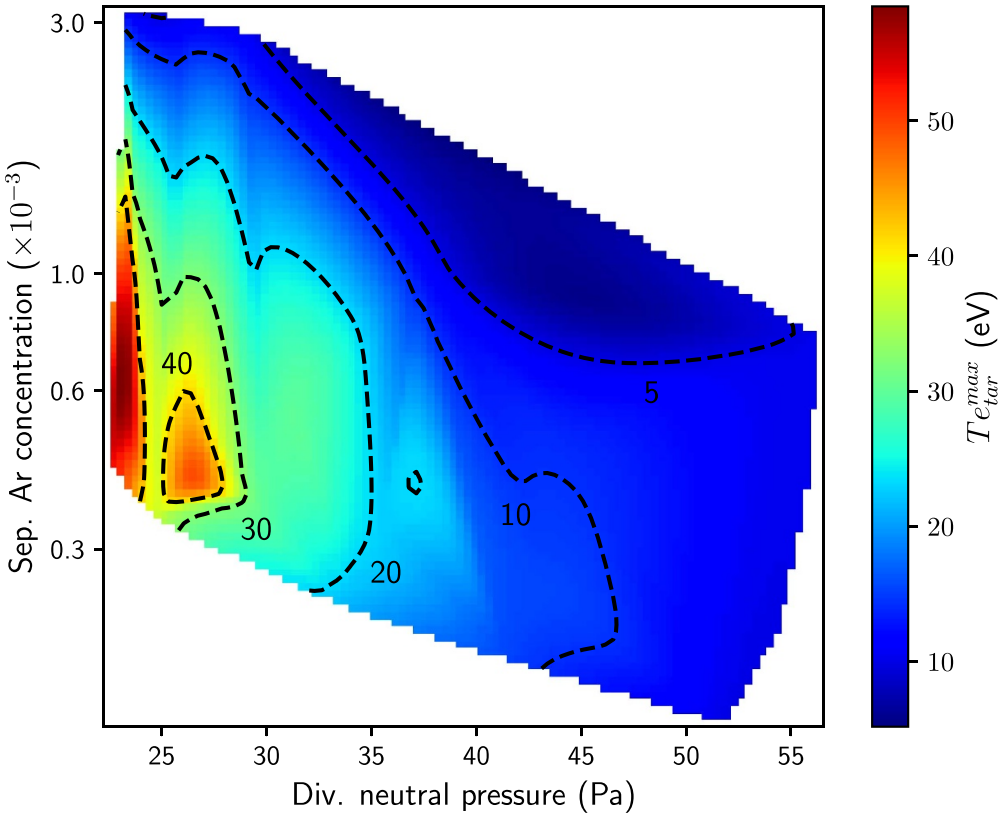

Figure 5. Maximum outer target electron temperature (eV).

It would then be doubtful to extract definite hard boundaries from such a study, but the qualitative conclusions are very unlikely to be affected. To guide the eye, we also added contour plots at $10\,\mathrm{MW m^{-2}}$ end 5 eV, corresponding to the values usually considered acceptable for a feasible cooling system and reasonably low sputtering. The two figure shows that a possible operational space for the EU-DEMO divertor seems to exist, though the requirement on T_e is quite strict. This is a point worth deeper analysis.

Figures 6 and 7 give information on the influence of impurities on the overall edge power balance. Figure 6 shows the total power fraction dissipated in the edge. It sums up contributions from line radiation (mostly impurities), ionization (sustaining recycling processes) and bremsstrahlung (a minor contribution). The added contours help to identify regions with different dissipation levels. The picture assumes a total heating power:

$$P_{\mathrm{heat}} = P_{\alpha} + P_{\mathrm{aux}} \approx 450\,\mathrm{MW} \tag{2}$$

and it is accepted that the power not crossing the separatrix is dissipated by a proper core radiator. The picture highlights that less than 10% of the given power goes to the target without any mediating process. Most of it is either radiated in the edge/SOL, or needed to sustain the recycling regime. The high dissipation level means that most of the power reaches eventually the wall chamber in form of photons. Since they are not affected by the magnetic field, the resulting distribution will be relatively uniform. To provide a rough number, we evaluated the average wall heat load obtained assuming purely isotropic distribution for the reference case discussed later in section 5, resulting in a rough estimate of $0.21\,\mathrm{MW m^{-2}}$.

If we focus on radiation in the SOL (i.e. mostly on the effect of Ar), the situation is somehow different, as detailed in figure 7. It shows the radiation fraction, evaluated including only line radiation processes taking place in the SOL (which can be ascribed almost completely to the Ar impurity), and takes as reference the power P_{sep} crossing the separatrix. Comparative analysis of figures 6 and 7 suggest that, although needed to guarantee sufficient target power mitigation, a SOL radiator like Ar will contribute only a minor correction on the overall edge power balance. Notice also that, as the Ar concentration increases, the power radiation distribution shifts more towards the core region, lowering SOL radiation fraction. We observe that, since most of the power balance will be dominated by the core radiator, it would be advisable, at a further stage of the design process, to extend the current work by explicitly including an additional impurity species.

Radiative processes distribute uniformly the power load onto the outer wall, lowering the overall target peak power density. Energy dissipation induced by ionization is much less effective, since the potential energy is still transported along the magnetic field lines by plasma convection, and ultimately released to the target plates through surface recombination. However, it does contribute significantly to local plasma cooling, and help creating favorable detachment conditions. This is made obvious by figure 8, which shows the ratio of electron pressure at the outer target to the X-point. By comparing it with

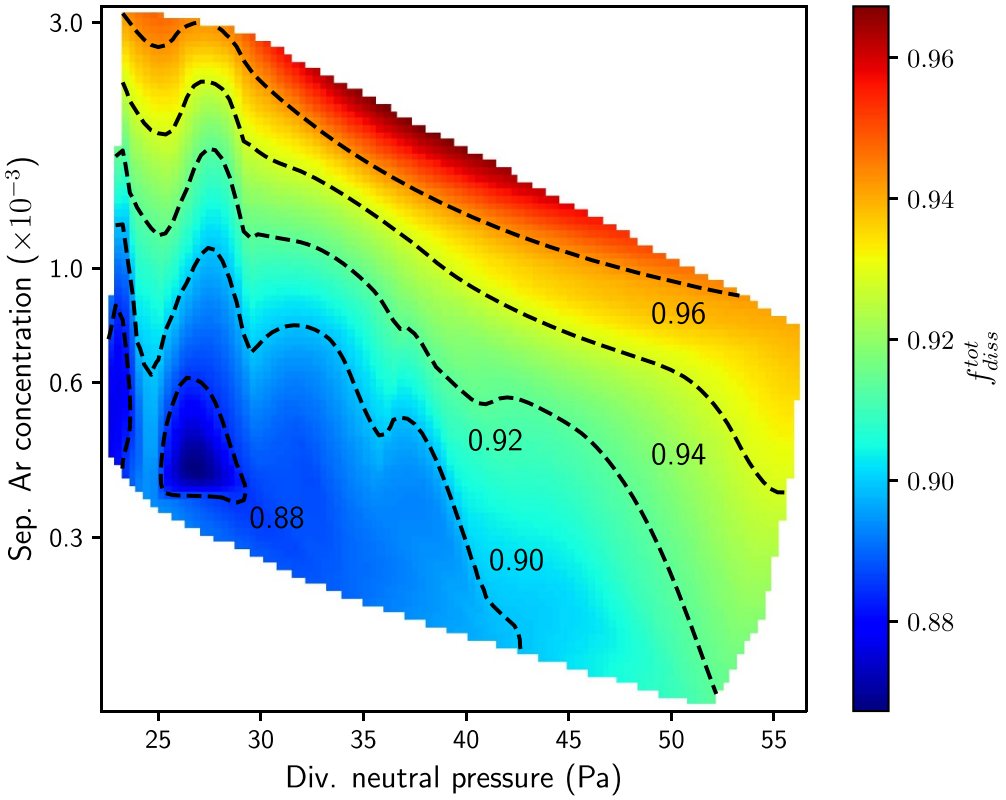

Figure 6. Dissipated power total fraction. It includes both radiative processes (line radiation, bremsstrahlung), and the power needed to feed recycling processes. It is evaluated taking as reference the total heating $P_{\text{heat}} \approx 450\,\text{MW}$.

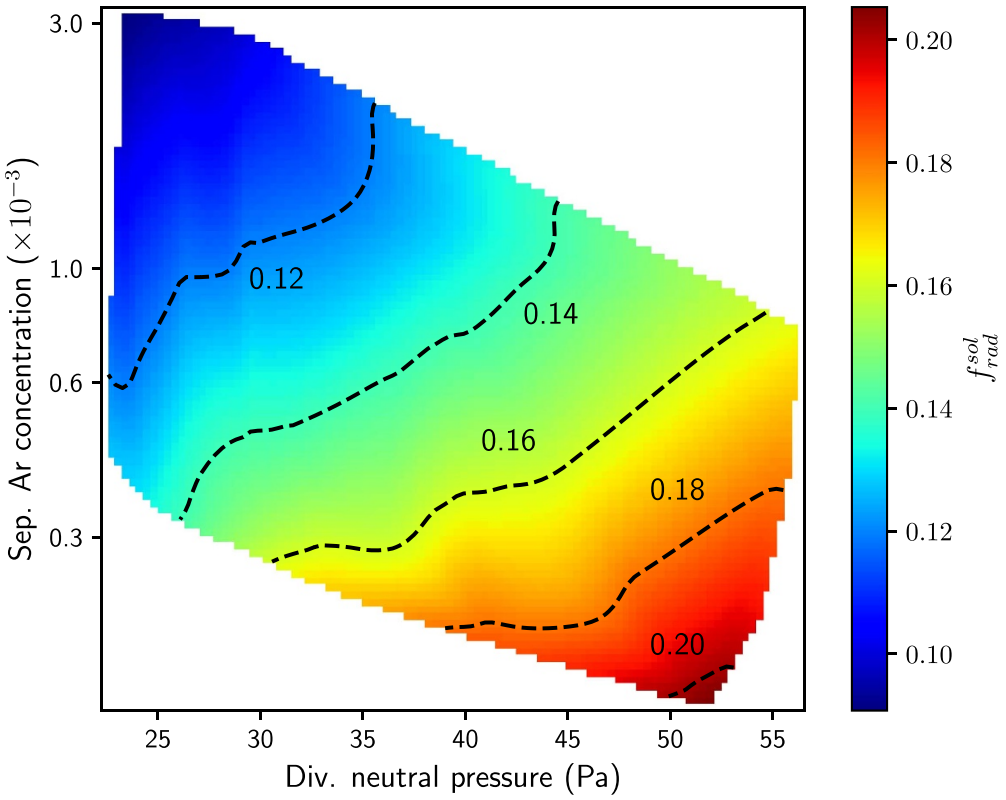

Figure 7. Radiation SOL fraction. It includes only line radiation processes, and takes as reference the power crossing the separatrix $P_{\text{sep}} \approx 130\,\text{MW}$.

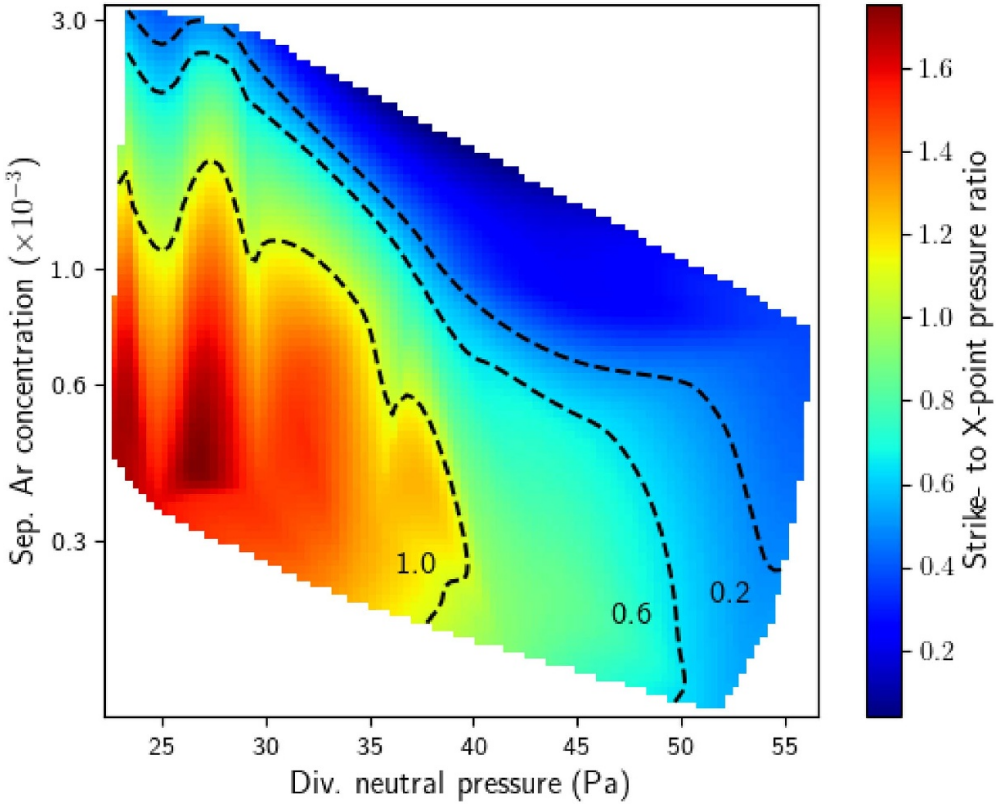

Figure 8. Outer strike- to *X*-point electron pressure ratio.

figures 6 and 7 we can immediately observe the much stronger correlation of this ratio with the map of power dissipation, as opposed to radiation.

We consider now the presence of impurities in the plasma. Figure 9 shows the $Z_{\rm eff}$ value averaged at the separatrix, that we use here as a proxy for the core value. It shows a relatively clean plasma, with $Z_{\rm eff}$ significantly departing from 1.0 only in the region of low density/high impurity seeding. On the other hand, we should remember that the present analysis only accounts for He and Ar, while the actual list of present impurities can be much wider (e.g. W and a core radiator like Xe will likely give a contribution). At present, it is hard to assess what effect such additional elements could actually have; we plan to include them in later extended studies. Finally, figure 10 shows the He compression in the divertor, defined as ([25]):

$$C_{\rm He} = \frac{n^{\rm div}_{0,\rm He}}{n^{\rm core}_{z,\rm He}} \tag{3}$$

with $n^{\rm div}_{0,\rm He}$ referring to neutrals and $n^{\rm core}_{z,\rm He}$ to the ions. Values shown in the figure are quite low, not reaching 2%. It should be observed, however, that neutrals usually accumulate in the divertor and sub-divertor, which is only partially included in our fluid simulations. Moreover, the geometrical details of the vessel wall play an important role. In the future, fully kinetic studies, with better atomic physics description for the impurities (which do not take advantage yet of the AFN approach) and accurate divertor region geometry will be required.

To close the analysis of the EU-DEMO operational space, it is interesting to gather in a single place the acceptable boundaries determined by the individual criteria previously considered. Figure 11 shows contours for relevant levels of target electron temperature, $Z_{\rm eff}$ at the separatrix, and target peak heat flux density. As background for the data, we selected the map of a critical quantity like the electron temperature, already shown in figure 5. It appears immediately that, of the three criteria compared, the one on the peak target heat flux is the least stringent. In fact, the main driver reducing the power to target is the addition of impurities, and we can see that load decreases as the separatrix Ar concentration rises. A similar trend is observed, as expected, for the target temperature. However, this second criterion appears to be noticeably more stringent than the power one. It is also interesting to observe how temperature variation and the $Z_{\rm eff}$ separatrix level have dangerously opposite trends. As expected, with increasing Ar separatrix concentration the core $Z_{\rm eff}$ value increases, opposite to the two other criteria. Moreover both changes from $Z_{\rm eff} = 1.4$ to $Z_{\rm eff} = 1.2$ and then to $Z_{\rm eff} = 1.1$ correspond to a dramatic reduction of the available operational space extension. Accumulation inside the separatrix depends on details of core transport, which an edge code like SOLPS-ITER can only partially account for. The critical influence we observe of the maximum $Z_{\rm eff}$ level on the operational space amplitude should stimulate efforts to develop in the future integrated edge-core modeling studies.

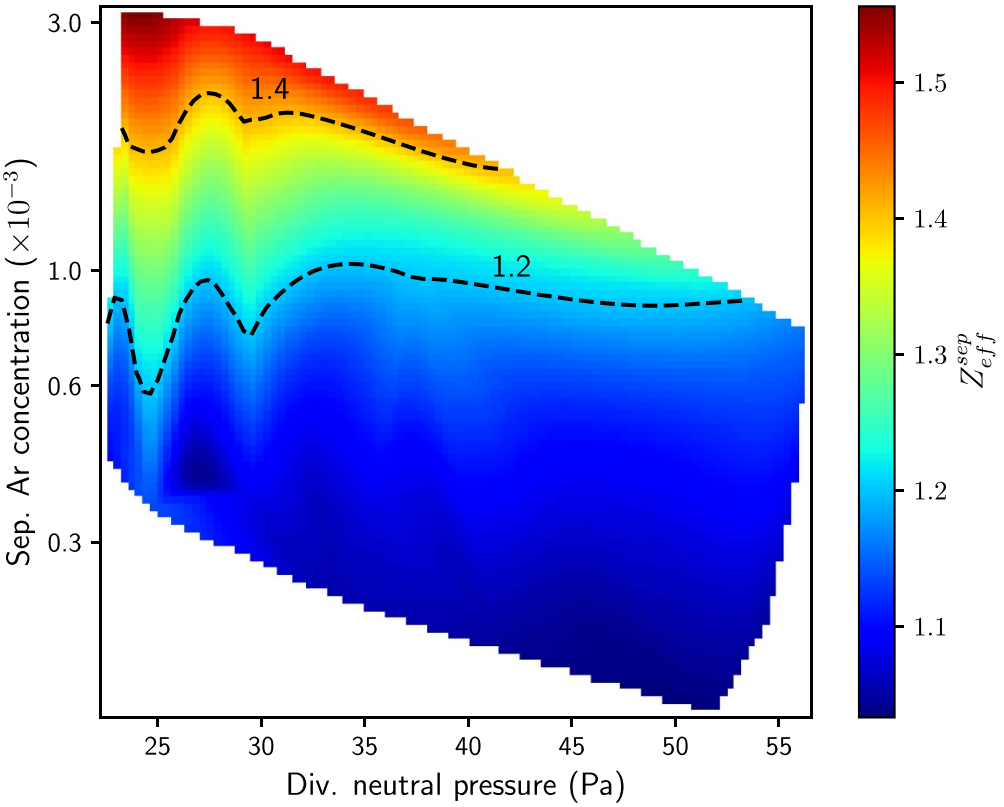

Figure 9. Z_{eff} averaged along the separatrix.

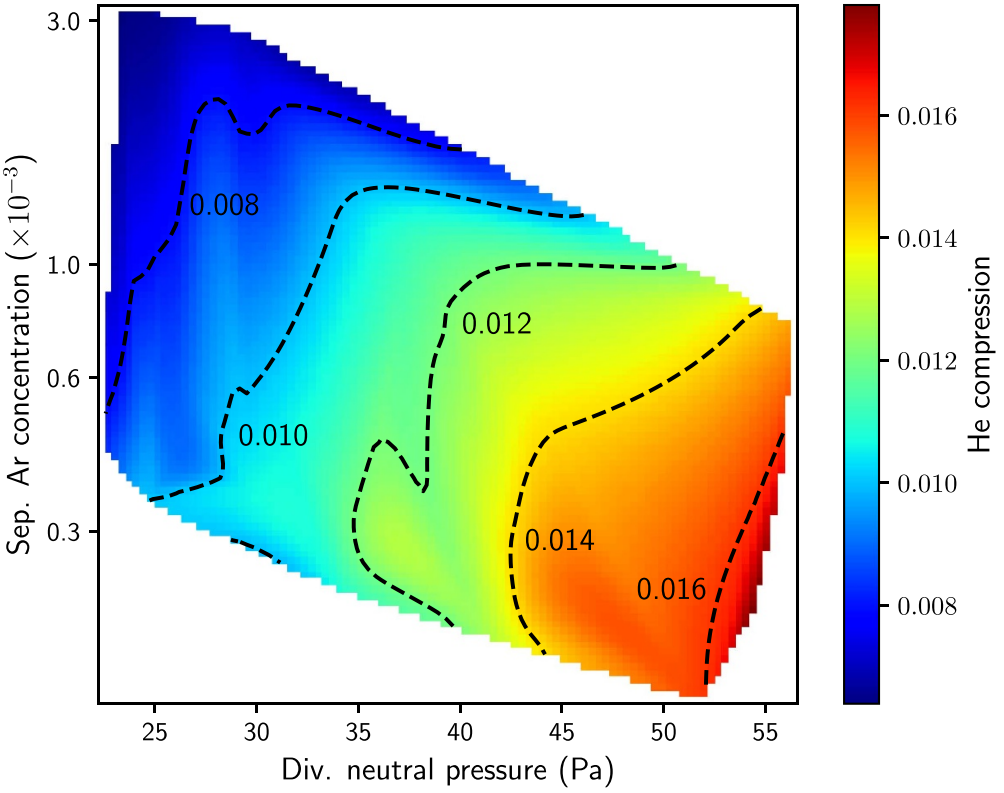

Figure 10. Helium compression in the divertor.

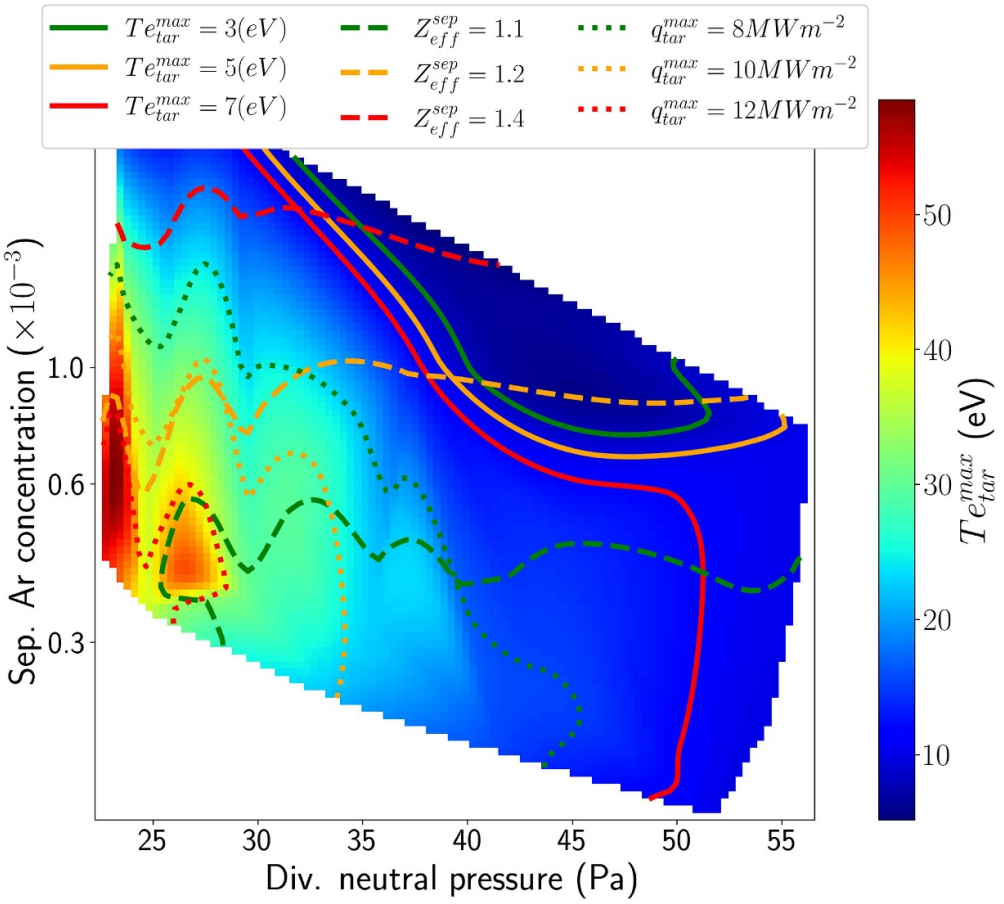

Figure 11. Comparison of various constraints in the operational space.

5. Detailed study

In this section we present in more detail the results of a specific run. This corresponds to divertor neutral pressure $p_{0,\mathrm{div}} = 45.0\,\mathrm{Pa}$ and Ar separatrix concentration $c_{\mathrm{Ar,sep}} = 4.4 \times 10^{-4}$. For this run, the peak power deposition at the outer target is $q_{\mathrm{max}} = 6.6\,\mathrm{MWm}^{-2}$ and the maximum electron temperature (outer plate) is $T_{\mathrm{e,max}} = 9.6\,\mathrm{eV}$. We selected this specific case because (i) it shows acceptable target heat flux density (including some margin on the conventional $10\,\mathrm{MWm}^{-2}$) and (ii) it is not adjacent to the operational space boundary.

Figures 12 and 13 show the electron temperature and density in the divertor region. Comparing the two maps makes it clear how the inner target, cold and with large density, is detached, while at the outer condition is less clear. To better appreciate the inner target details, an inset has been put in figure 12, with linear color scale and saturation at 10 eV. This shows how, right at the inner target, the electron temperature stays well below 4 eV. Figure 14 compares the electron pressure radial profiles along the divertor entrance and at the outer target. If we take it as a proxy for detachment, we conclude that only the innermost ≈2 cm from the separatrix show a significant detachment marker. Further away, the plasma re-attaches. Consistently, the radial temperature profiles at the outer target, reported in figure 15 show that when the pressure drop fades away also the electron temperature rises to the relatively large value ≈8 eV. In fact, it can be observed that such T_{e} level is significantly larger than the value often considered triggering substantial pressure drops (3–5 eV). This may be an indication that friction is not the only active mechanism here; radial transport may contribute to divert momentum towards the private flux region. We also observe that no target profiles beveling is considered in this study. Proper plates shaping will certainly be introduced in later, more refined designs. This will certainly contribute to optimize target plasmas parameters, likely resulting in a more extended detached region. When remapped to upstream conditions, the detachment region extension reduces down to a few mm, i.e. comparable with the expected power decay length. Checking other runs in the available simulation database (not shown here), we did find a higher pressure drop close to the separatrix, but the detached region width did not vary appreciably. Though previous studies have already suggested that the outer divertor may likely only partially detach [7], we found such short extension a bit surprising; this will likely be subject of future investigations.

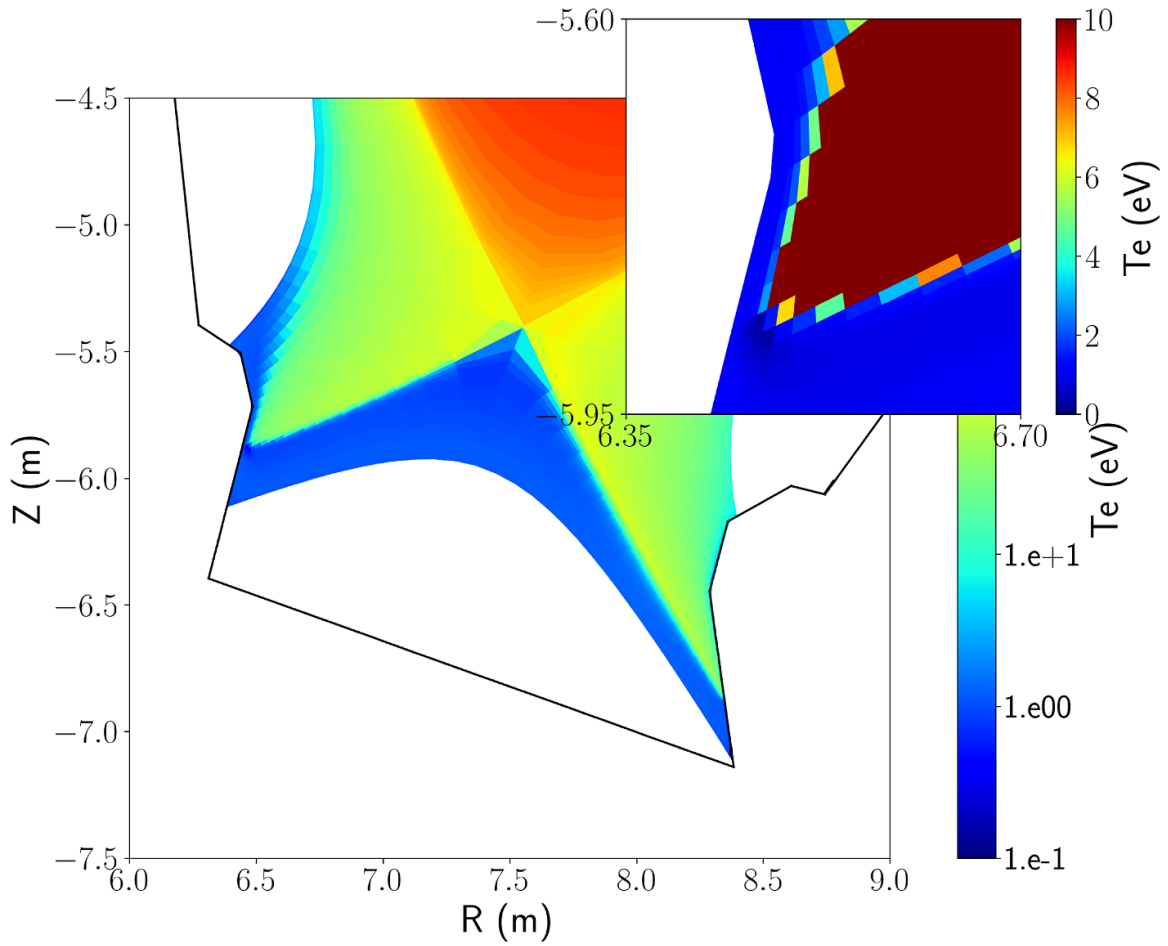

Figure 12. Electron temperature in the divertor region (eV). The upper-right inset zooms on the inner strike point region.

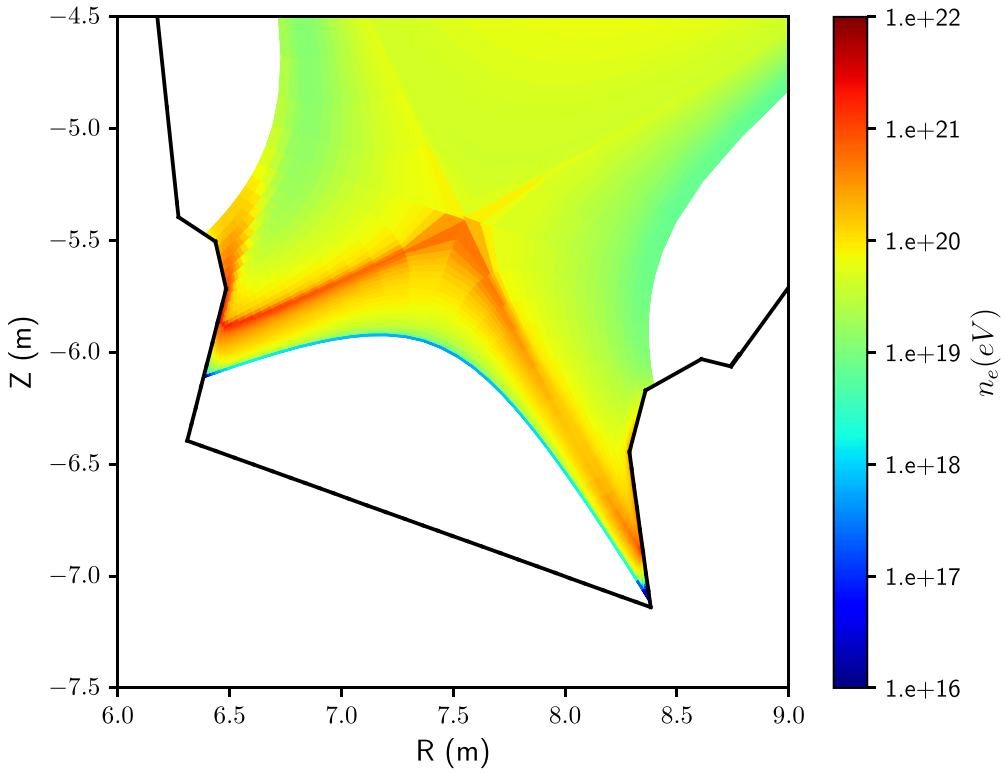

Figure 13. Electron density in the divertor region (m^{-3}).

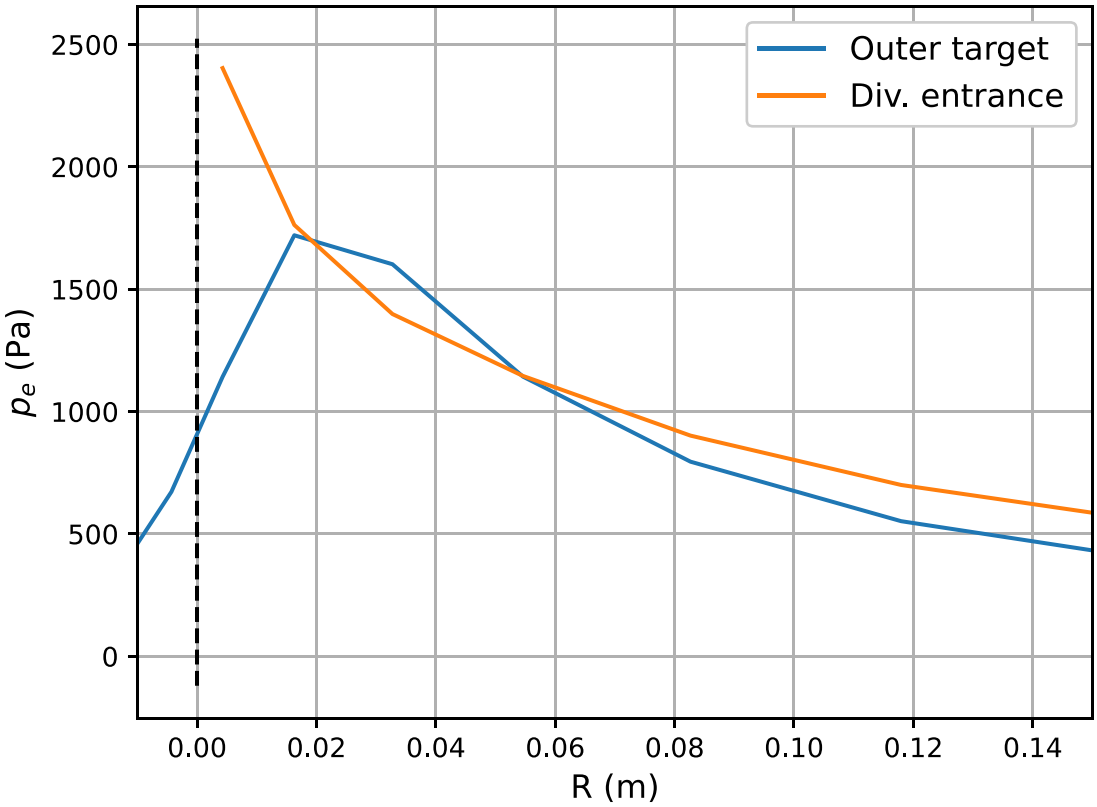

Figure 14. Electron pressure (Pa) at the outer divertor entrance and target.

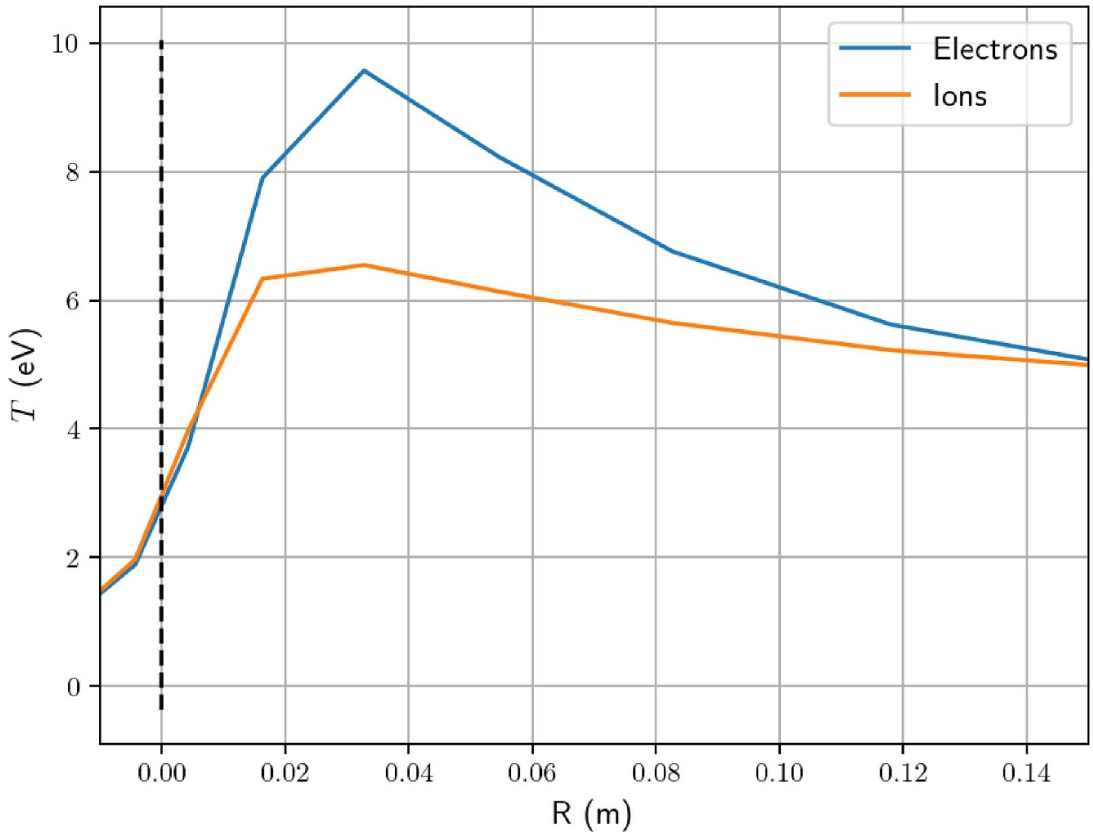

Figure 15. Electron and ion radial temperature (eV) profiles along the outer target.

6. Conclusions and perspectives

In this work we presented an extensive analysis of the EU-DEMO operating conditions produced with the SOLPS-ITER code. It leverages some recently introduced features, such as the AFN model for the main neutral species to accelerate convergence. Also, several others, more consolidated simplifying features are exploited, the most impacting being probably not including drifts in our simulations. We aimed at determine if it is possible to operate the EU-DEMO divertor in a safe way, and possibly to have a first look at the compatibility of such operation with acceptable core performances.

We assumed divertor detachment to be favored by injecting some extrinsic impurity. Ar was selected as SOL radiator. It is commonly acknowledged that also a higher Z core impurity will be needed, but we did not include it in our current study. Alternatively, it may be speculated that even a low W content, which unavoidably will penetrate from the wall surface, could provide at least some of the required additional radiation. We did find evidence of a possible finite-extension divertor operation region, which can be obtained at marginally acceptable upstream density (up to $\approx 0.7\, n_{\mathrm{GW}}$). Also, the Ar core concentration is relatively reduced, leaving some space for core radiators to be included in further studies. Our work suggests the inner divertor to be robustly detached, while the outer one enters easily the high-recycling regime but does not detach, except perhaps very close to the separatrix. While this seems to be still safe in terms of target heat flux, the full implications of this finding need to be clarified by further work, which should also focus more specifically on the possibility to enter a significantly detached regime.

We believe the current work naturally points to a few extensions. First, it would be desirable to perform more detailed analyses, at least for a few points within the identified operational space, e.g. by including drifts and the details of the wall geometry. This would allow assessing critical information like the details of the wall loads and sputtering rates. Also, we wish to take in more precise core transport modeling, to eventually include realistically a core radiator in our study. An accurate core transport model could justify the additional computational resources required by adding to the study a relatively large Z element like Xe. Moreover, this would also improve the evaluation of impurity accumulation in the confined plasma, which may impact the EU-DEMO operational space extension. All data files and python scripts used to produce the analysis and figure presented in this paper are available on Zenodo at the doi: https://doi.org/10.5281/zenodo.14 894 868.

Acknowledgments

This work has been carried out within the framework of the EUROfusion Consortium, funded by the European Union via the Euratom Research and Training Programme (Grant Agreement No. 101052200 - EUROfusion). Views and opinions expressed are however those of the author(s) only and do not necessarily reflect those of the European Union or the European Commission. Neither the European Union nor the European Commission can be held responsible for them. High-performance computing resources were provided by the EUROfusion and performed at the High-Performance Computers Eurofusion-Gateway (Bologna, Italy).

References

[1] Wenninger R. *et al* 2017 The demo wall load challenge *Nucl. Fusion* **57** 046002
[2] Pitts R.A. *et al* 2019 Physics basis for the first ITER tungsten divertor *Nucl. Mater. Energy* **20** 100696
[3] Subba F., Coster D.P., Juanes A.N.E., Fable E., Wenninger R. and Zanino R. 2018 Analysis of highly radiative scenarios for the EU-DEMO divertor target protection *Contrib. Plasma Phys.* **58** 758–64
[4] Affinito L. *et al* DTT divertor tokamak test facility interim design report (available at: www.dtt-project.it/DTT_IDR_2019_WEB.pdf)
[5] Aho-Mantila L. *et al* 2021 Scoping the characteristics and benefits of a connected double-null configuration for power exhaust in EU-DEMO *Nucl. Mater. Energy* **26** 100886
[6] Xiang L., Militello F., Moulton D., Subba F., Aho-Mantila L., Coster D., Wensing M., Lunt T., Wischmeier M. and Reimerdes H. 2021 The operational space for divertor power exhaust in DEMO with a super-x divertor *Nucl. Mater. Energy* **61** 076007
[7] Subba F., Coster D.P., Moscheni M. and Siccinio M. 2021 SOLPS-ITER modeling of divertor scenarios for EU-DEMO *Nucl. Fusion* **61** 106013
[8] Wiesen S. *et al* 2021 The new SOLPS-ITER code package *J. Nucl. Mater.* **463** 480–4
[9] Martin Y.R. and Takizuka T. 2008 (the ITPA CDBM H-mode Threshold Data Group) Power requirement for accessing the H-mode in ITER *J. Phys.: Conf. Ser.* **123** 012033
[10] Maviglia F. *et al* 2021 Impact of plasma-wall interaction and exhaust on the EU-DEMO design *Nucl. Mater. Energy* **26** 100897
[11] Siccinio M., Federici G., Kembleton R., Lux H., Maviglia F. and Morris J. 2019 Figure of merit for divertor protection in the preliminary design of the EU-DEMO reactor *Nucl. Fusion* **59** 106026
[12] Wenninger R.P. *et al* 2014 DEMO divertor limitations during and in between ELMs *Nucl. Fusion* **54** 114003
[13] Van Uytven W., Dekeyser W., Blommaert M., Carli S. and Baelmans M. 2022 Assessment of advanced fluid neutral models for the neutral atoms in the plasma edge and application in ITER geometry *Nucl. Fusion* **62** 086023
[14] Dekeyser W. *et al* 2021 Plasma edge simulations including realistic wall geometry with SOLPS-ITER *Nucl. Mater. Energy* **27** 100999
[15] Vervloesem N., Dekeyser W., van den Kerkhof S. and Baelmans M. 2024 Error based grid adaptation methods for plasma edge simulations with SOLPS ITER *Contrib. Plasma Phys.* **64** e202300126
[16] Kaveeva E., Rozhansky V., Senichenkov I., Veselova I., Voskoboynikov S., Sytova E., Bonnin X. and Coster D. 2018 Speed-up of SOLPS-ITER code for tokamak edge modeling *Nucl. Fusion* **58** 126018
[17] Akkermans G.R.A., Classen I.G.J., Perillo R., van der Meiden H.J., Federici F. and Brezinsek S. 2020 The role of hydrogen molecular effects on detachment in Magnum-PSI *Phys. Plasmas* **27** 102509
[18] Saito S., Nakamura H., Sawada K., Hoshino K., Kojima Y., Doi T., Kobayashi M., Hasuo M., Homma Y. and Yamoto S. 2018 Emission of high rovibrational hydrogen molecules

under detached plasma conditions by recycling on the tungsten wall *Nucl. Fusion* **64** 126067
[19] Kaveeva E. *et al* 2020 SOLPS-ITER modelling of ITER edge plasma with drifts and currents *Nucl. Fusion* **60** 046019
[20] Brida D., Silvagni D., Eich T., Faitsch M. and McCarthy P. 2020 Role of electric currents for the SOL and divertor target heat fluxes in ASDEX Upgrade *Plasma Phys. Control. Fusion* **62** 105014
[21] Rozhansky V., Kaveeva E., Senichenkov I., Sorokina D., Vekshina E., Coster D., McCarthy P. and Khromov N. 2020 Currents structure in the scrape-off layer of a tokamak *Nucl. Mater. Energy* **25** 100840
[22] Eich T., Goldston R.J., Kallenbach A., Sieglin B. and Sun H.J. 2018 Correlation of the tokamak H-mode density limit with ballooning stability at the separatrix *Nucl. Fusion* **58** 034001
[23] Varoutis S., Tantos C., Strobel H., Day C., Dhard C.P., Haak V., Igitkhanov Y. and Naujoks D. 2024 Numerical simulation of neutral gas dynamics in the W7-X sub-divertor *Nucl. Fusion* **64** 076011
[24] Tantos C., Varoutis S., Hauer V., Day C. and Innocente P. 2023 3D numerical study of neutral gas dynamics in the DTT particle exhaust using the DSMC method *Nucl. Fusion* **64** 016019
[25] Goetz J.A., Lipschultz B., Pitcher C.S., Terry J.L., Bonoli P.T., Rice J.E. and Wukitch S.J. 1999 Impurity compression and enrichment studies on alcator C-Mod *J. Nucl. Mater.* **266–269** 354–9